NASA TECHNICAL NOTE

NASA TN D-6565

CHARACTERISTICS OF THE OPTICAL RADIATION FROM KAUFMAN THRUSTERS

by Nelson L. Milder and James S. Sovey

Lewis Research Center
Cleveland, Ohio 44135

NATIONAL AERONAUTICS AND SPACE ADMINISTRATION • WASHINGTON, D. C. • NOVEMBER 1971

1. Report No.	2. Government Accession No.	3. Recipient's Catalog No.
NASA TN D-6565		

4. Title and Subtitle	5. Report Date
CHARACTERISTICS OF THE OPTICAL RADIATION FROM KAUFMAN THRUSTERS	November 1971
	6. Performing Organization Code

7. Author(s)	8. Performing Organization Report No.
Nelson L. Milder and James S. Sovey	E-6469
	10. Work Unit No. 113-26

9. Performing Organization Name and Address	11. Contract or Grant No.
Lewis Research Center National Aeronautics and Space Administration Cleveland, Ohio 44135	
	13. Type of Report and Period Covered
12. Sponsoring Agency Name and Address	Technical Note
National Aeronautics and Space Administration Washington, D.C. 20546	14. Sponsoring Agency Code

15. Supplementary Notes

16. Abstract

The optical radiation from plasma discharges of electron-bombardment mercury-ion thrusters was investigated. Spectrographic measurements indicated that the discharge was composed primarily of mercury atoms and singly charged ions. Excitation spectra of doubly charged mercury ions was measured to obtain the fraction of such ions in the discharge. Accomplishments of spectroscopic measurements of a hollow cathode thruster included the identification of two diagnostic lines in the mercury spectrum and the interpretation of the spectral amplitudes in terms of a superposition of primary and Maxwellian electron distributions. Potential application of optical techniques to thruster control applications was also suggested by the measurements.

17. Key Words (Suggested by Author(s))	18. Distribution Statement
Optical radiation; Spectral line amplitudes; Electron collisional excitation; Thruster diagnostics; Mercury bombardment thrusters; Mercury ions; Mercury atoms	Unclassified - unlimited

19. Security Classif. (of this report)	20. Security Classif. (of this page)	21. No. of Pages	22. Price*
Unclassified	Unclassified	35	$3.00

* For sale by the National Technical Information Service, Springfield, Virginia 22151

CHARACTERISTICS OF THE OPTICAL RADIATION FROM KAUFMAN THRUSTERS

by Nelson L. Milder and James S. Sovey

Lewis Research Center

SUMMARY

The optical radiation from plasma discharges of electron-bombardment mercury-ion thrusters was investigated. The purpose of the investigation was to determine the applicability of spectroscopic diagnositc measurements to such thrusters. To accomplish this task, a spectrograph was used to determine the atomic and ionic species in the discharge plasma of a 30-centimeter-diameter hollow cathode thruster and a 1.5-meter-diameter thermionic cathode thruster. A 0.5-meter Ebert mounted optical monochromator was used to study spectral line intensity of radiation emanating from the discharge of the 30-centimeter-diameter thruster.

The results of these measurements indicated that the discharge was composed primarily of mercury atoms and singly charged ions. Excitation spectra of doubly charged mercury ions was also detected in both the 30-centimeter- and the 1.5-meter-diameter thrusters.

Diagnostics performed on the 30-centimeter hollow cathode thruster resulted in (1) a theoretical interpretation of the observed spectra in terms of a superposition of primary electrons upon a Maxwellian distribution and (2) the identification of two mercury atom lines at 365.5 and 365.0 nanometers (3655 and 3650 Å) that were suitable for application of line amplitude ratioing techniques. The spectroscopic measurements indicated that electron temperatures in the discharge plasma ranged from about 1.2 to 7.5 electron volts depending on discharge voltage and radial location. Also, the primary electron (defined as the ratio of primary electron density to Maxwell density) varied from near zero at three-quarters radius to about 5 percent on the thruster axis.

Spectral line amplitude measurements in the neutralizer region indicated a neutralizer-beam coupling voltage of about 20 to 22 volts, in qualitative agreement with probe measurements of this potential for neutralizers operating in spot mode. These results suggest possible use of spectroscopic measurements to thruster control applications by correlating detectable varying optical effects with changing thruster performance.

The percentage of doubly ionized mercury with respect to the atom density in the discharge could be measured directly and was found to be a maximum of about 2 percent on the thruster axis for a discharge voltage of 58 volts, dropping to about 1.3 percent at half radius. At lower discharge voltages, the ratio of double ions to neutral atoms did not exceed about 0.8 percent.

INTRODUCTION

The purpose of this investigation was to determine if spectroscopic diagnostic measurements could be made in mercury bombardment thrusters. The discharge plasma in the ion chamber of a mercury-electron bombardment thruster is formed primarily by the collision of monoenergetic and thermal electrons with mercury atoms. Phenomenological descriptions of the plasma have been given elsewhere (refs. 1 and 2). In general, the plasma electron densities in such thrusters are of the order of 10^{10} to 10^{11} per cubic centimeter (refs. 3 and 4). Maxwellian electron temperatures generally do not exceed about 10 electron volts (ref. 4), and the neutral atom density is estimated to be of the order of 10^{12} per cubic centimeter (ref. 3). The values of these quantities vary with thruster size and operating conditions. The ionization produced by electron bombardment is accompanied by collisional excitation of the atomic and ionic species in the discharge. Decay of these excitations produces radiation, as a visual inspection of an operating thruster immediately reveals. The present work describes investigations of this radiation and extends the results of our preliminary measurements (ref. 5).

There are several motivations for using spectroscopic techniques to study thruster plasmas. Previous diagnostics of the discharge have been based almost entirely on Langmuir probe measurements (refs. 1 and 2). Although these measurements have yielded plasma density, potential, and electron temperature profiles, there is always the concern that electric probes can introduce local disturbances that affect the parameters being measured. Spectroscopy is a diagnostic method that does not disturb the plasma.

In addition, there are properties of the thruster plasma that are particularly conducive to spectroscopic analysis. The low particle density in the discharge yields a plasma that is optically thin except for resonant states. This means that the radiation emanating from processes occurring deep within the plasma volume can be observed. Thrusters can be maintained at a steady operating condition for long times compared with those needed to obtain spectra. The operating point can be readily changed to another stable condition, so that the effect of varying thruster parameters on the radiative processes can be studied in detail.

There are limitations, however. Data interpretation is generally not direct, requiring a knowledge of or assumptions on the nature of the physical processes in the discharge producing the radiation. Accurate measurements require detailed information on the optical properties of the radiating atom. Often such information is not available for heavy atoms such as mercury. Also, because the emitted light emanates from atomic sources located along the line-of-sight of the detecting system, local properties of the discharge plasma cannot easily be measured. Thus, one generally obtains infor-

mation on the average properties of the discharge. Even with these restrictions it was found that data could be interpreted in terms of a physical model to be described herein.

EXPERIMENTAL APPARATUS AND PROCEDURE

Thrusters

The 30-centimeter- and the 1.5-meter-diameter thrusters used in this study are shown schematically in figures 1 and 2. Detailed descriptions of the 30-centimeter thruster have been given in references 6 and 7. In this thruster a hollow cathode serves as the source of ionizing electrons. These electrons are contained in the discharge chamber by means of field-shaping permanent magnets. Propellant utilization ranged from about 80 to 95 percent. (The 30-cm thruster was operated by V. K. Rawlin and R. T. Bechtel of Lewis for this investigation.)

The 1.5-meter (anode) diameter thruster (ref. 8) uses 10 oxide-coated thermionic emitters to produce ionizing electrons. A very weak magnetic field (of the order of

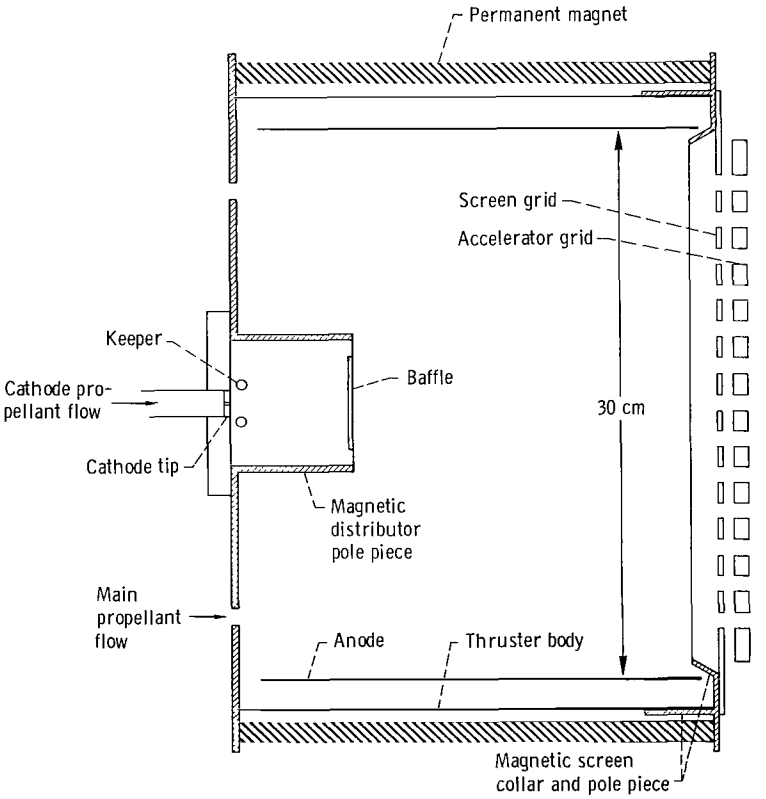

Figure 1. - Section view of a 30-centimeter-diameter thruster.

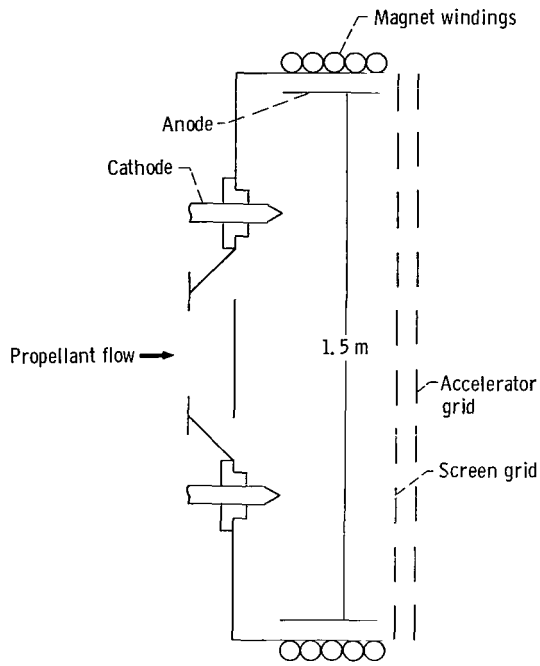

Figure 2. - Section view of 1.5-meter-diameter thruster.

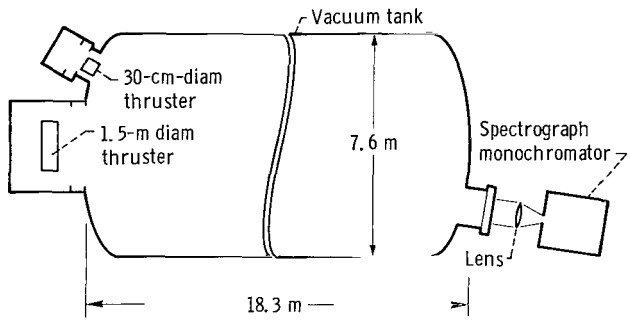

Figure 3. - Experimental arrangement.

10^{-4} T) provided the means for suppressing electron radial diffusion to the anode. Propellant utilization was nominally 65 percent. (This thruster was operated by S. Nakanishi of Lewis.)

Facility

The thrusters were run in the Lewis Research Center 7.6-meter-diameter by 18.3-meter long vacuum facility described in reference 9. Their position in the vacuum tank is shown in figure 3. Facility constraints required that the optical detectors be

located at the opposite end of the facility from the thrusters. This meant that the discharge chamber was viewed through the ion exhaust beam. Radiation emanating from regions downstream of the discharge chamber would be due to neutralizing electron-atom excitations, electron-ion recombination, and possibly charge exchange. The downstream radiation was measured and found to represent only a negligible fraction of the total measured radiation.

Optical Measurements

Two optical detection systems were used. A spectrograph using photographic plates was useful for general surveys of the thruster spectrum and for excited species identification. This system is particularly useful for detecting very weak transitions. A monochromator with a photomultiplier detector was used for quantitative measurements of individual spectral lines.

Spectrograph. - A plane grating spectrograph of a Czerny-Turner design with 3/4-meter focal length was used. The spectrograph was equipped with a cassette for holding 12.7- by 17.8-centimeter photographic glass plates. The cassette could be positioned by means of a vertical rack, so that several spectra could be obtained on a single plate. A mechanical shutter at the entrance slit was used to obtain exposure times ranging from 1/200 second to several seconds.

The range of wavelengths studied was from 230 to 670 nanometers (2300 to 6700 Å), with a dispersion varying linearly from 2.1 nanometers per millimeter (21 Å/mm) at 370 nanometers (3700 Å) to 1.93 nanometers per millimeter (19.3 Å/mm) at 630 nanometers (6300 Å). The best resolution obtained at this range of dispersion was of the order of 0.15 nanometers (1.5 Å). The high speed (f/6.3) of the instrument was especially useful in obtaining spectra of the 30-centimeter-diameter thruster. The long distance between this plasma source and spectrograph entrance slit resulted in many lines having rather low intensity. A typical densitometer trace of photographed spectral lines is shown in figure 4.

Monochromator. - An Ebert mounted, plane grating monochromator with a 0.5-meter focal length was used to study discrete spectral line amplitudes. The instrument dispersion was 3.2 nanometers per millimeter (32 Å/mm). The plane grating was rotated to cover the wavelength range from 230 to 800 nanometers (2300 to 8000 Å). The recorded photomultiplier signal was corrected for the spectral response of the optical system. This response was determined using a radiance standard calibrated by the National Bureau of Standards.

The monochromator was used to obtain radial profiles of the 30-centimeter-diameter thruster. The procedure consisted of setting the monochromator on the peak

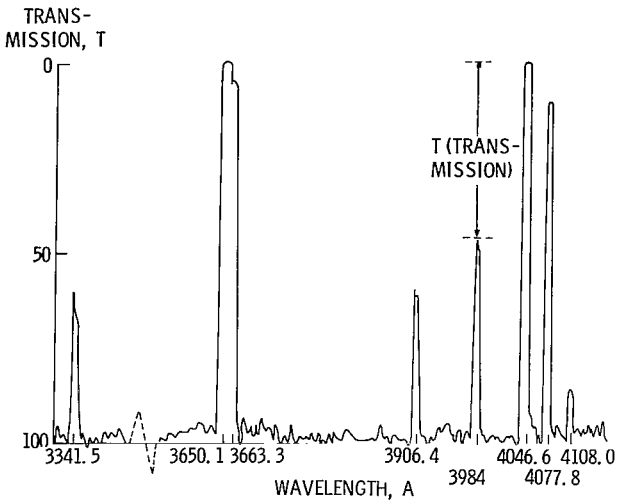

Figure 4. - Densitometer trace of spectral lines.

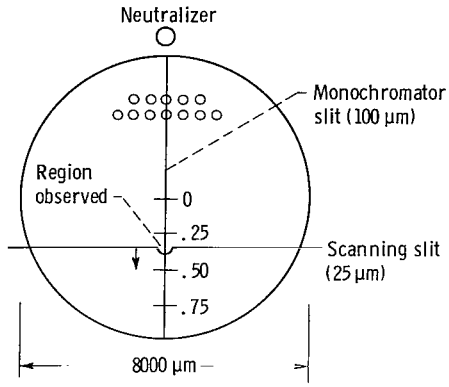

Figure 5. - 30-Centimeter-diameter thruster image viewed from downstream of the extraction grids.

of a given spectral line. A motor driven 25-micrometer horizontal slit was then used to scan the image on the vertical entrance slit of the monochromator as shown in figure 5. In this manner the area of thruster cross section observed represented about 0.005 percent of the total thruster cross sectional area. For measurements of the thruster discharge chamber plasma, profiles were obtained along the radial direction away from the neutralizer location.

SPECIES IDENTIFICATION AND OBSERVED LEVEL EXCITATIONS

A tabulation of most of the observed Hg I and Hg II transitions are given in tables I and II, respectively. Also given are the energies above ground state of the upper levels of the transitions. Identification was based on compilations given in the literature (refs. 10 to 14). Energy level diagrams are given in figures 6 and 7.

The mercury atom contains 80 electrons in the configuration

$$1s^2 2s^2 2p^6 3s^2 3p^6 3d^{10} 4s^2 4p^6 4d^{10} 4f^{14} 5s^2 5p^6 5d^{10} 6s^2$$

TABLE I. - OBSERVED Hg I SPECTRA

Series		Transition (ref. 15)	Wavelength, nm (ref. 13)	Upper state level, eV
Singlet	^1S	$8^1S_0 - 6^1P_1$	491.60	9.23
		$9^1S_0 - 6^1P_1$	410.80	9.73
		$10^1S_0 - 6^1P_1$	380.17	9.46
	^1P	$8^1P_1 - 7^1S_0$	671.62	9.55
		$9^1P_1 - 7^1S_0$	623.44	9.92
		$10^1P_1 - 7^1S_0$	580.36	10.05
		$11^1P_1 - 7^1S_0$	554.98	10.15
	^1D	$6^1D_2 - 6^1P_1$	579.06	8.86
		$7^1D_2 - 6^1P_1$	434.75	9.57
		$8^1D_2 - 6^1P_1$	390.64	9.90
		$9^1D_2 - 6^1P_1$	370.42	10.05
Singlet-triplet	$^{1,3}S$	$7^1S_0 - 6^3P_1$	407.78	5.15
		$9^3S_1 - 6^1P_1$	414.04	9.70
	^1P	$8^1P_1 - 7^3S_1$	607.26	4.55
		$9^1P_1 - 7^3S_1$	567.59	9.92
		$10^1P_1 - 7^3S_1$	531.67	10.05
		$11^1P_1 - 7^3S_1$	510.24	10.15
	^3P	$6^3P_1 - 6^1S_0$	253.65	4.89
	^3D	$6^3D_1 - 6^1P_1$	578.97	8.86
		$6^3D_2 - 6^1P_1$	576.96	8.86
		$7^3D_1 - 6^1P_1$	433.92	9.56
		$8^3D_2 - 6^1P_1$	390.19	9.90
Triplet	^3S	$7^3S_1 - 6^3P_0$	404.66	7.73
		$7^3S_1 - 6^3P_1$	435.84	7.73
		$7^3S_1 - 6^3P_2$	546.07	7.73
		$8^3S_1 - 6^3P_2$	334.15	9.18
		$8^3S_1 - 6^3P_0$	275.28	9.18
		$8^3S_1 - 6^3P_1$	289.36	9.18
		$9^3S_1 - 6^3P_2$	292.54	9.70
	^3P	$9^3P_0 - 7^3S_1$	587.20	9.86
		$9^3P_1 - 7^3S_1$	585.94	9.86
		$9^3P_2 - 7^3S_1$	582.15	9.87
		$10^3P_2 - 7^3S_1$	535.40	10.02
		$11^3P_2 - 7^3S_1$	512.05	10.15
		$12^3P_2 - 7^3S_1$	498.06	10.20
	^3D	$6^3D_1 - 6^3P_1$	313.15	8.85
		$6^3D_2 - 6^3P_1$	312.57	8.86
		$6^3D_1 - 6^3P_2$	366.29	8.86
		$6^3D_2 - 6^3P_2$	365.48	8.86
		$6^3D_3 - 6^3P_2$	365.01	8.86
		$6^3D_1 - 6^3P_0$	296.73	8.86
		$7^3D_2 - 6^3P_2$	302.35	9.56
		$7^3D_2 - 6^3P_1$	265.20	9.56
		$7^3D_3 - 6^3P_2$	302.15	9.56
		$8^3D_1 - 6^3P_2$	280.45	9.90
		$8^3D_3 - 6^3P_2$	280.35	9.90
		$9^3D_3 - 6^3P_2$	269.88	10.0

TABLE II. - OBSERVED Hg II SPECTRA

Wavelength, nm (ref. 14)	Transition (ref. 15)	Upper state level, eV	Wavelength, nm (ref. 14)	Transition (ref. 15)	Upper state level, eV
284.77	$7^2S_{1/2} - 6^2P_{3/2}$	11.9	448.75	----------	----
319.10	$9^2D_{3/2} - 7^2P_{1/2}$	17.3	460.66	$11^2P_{3/2} - 8^2S_{1/2}$	17.7
320.82	----------	----	466.03	$7^2D_{3/2} - 6^2P_{1/2}$	15.5
325.22	$10^2D_{5/2} - 7^2P_{3/2}$	17.7	470.46	$8^2G_{7/2,9/2} - 5^2F_{7/2}$	17.9
326.41	----------	----	476.22	$8^2G_{7/2} - 5^2F_{5/2}$	17.9
331.23	$D_{5/2} - {}^2P_{3/2}$	16.7	479.70	----------	----
338.52	----------	----	485.57	$9^2S_{1/2} - 7^2P_{3/2}$	16.4
345.17	----------	----	512.84	$7^2D_{5/2} - 6^2P_{3/2}$	15.4
349.83	$8^2D_{5/2} - {}^2P_{3/2}$	16.7	520.48	----------	----
352.42	$6^2F_{5/2} - 6^2D_{3/2}$	16.5	521.08	----------	----
353.26	----------	----	522.28	$7^2G_{7/2,9/2} - 5^2F_{7/2}$	17.6
354.94	----------	----	529.40	$7^2G_{7/2} - 5^2F_{5/2}$	17.6
359.35	$6^2F_{7/2} - 6^2D_{5/2}$	16.5	542.52	$5^2F_{5/2} - 6^2D_{3/2}$	15.3
360.58	$9^2D_{3/2} - 7^2P_{3/2}$	17.3	559.54	$5^2F_{5/2} - 6^2D_{5/2}$	15.3
377.63	$9^2S_{1/2} - {}^2P_{3/2}$	16.4	585.19	$6^2G_{7/2} - {}^2F_{5/2}$	17.2
383.93	----------	----	612.33	----------	----
398.40	$6^2P_{3/2} - 6^2D_{5/2}$	7.51	614.69	----------	----
417.80	----------	----	614.95	$7^2P_{3/2} - 7^2S_{1/2}$	13.9
421.25	$10^2G_{7/2,9/2} - 5^2F_{7/2}$	18.2	629.13	$6^2G_{7/2,9/2} - 5^2F_{7/2}$	17.2
422.73	----------	----	639.49	$6^2G_{7/2} - 5^2F_{5/2}$	17.2
439.86	$8^2D_{5/2} - 7^2P_{3/2}$	16.7	650.15	----------	----
442.52	$8^2D_{3/2} - 7^2P_{3/2}$	16.7	652.11	$8^2S_{1/2} - 6^2P_{3/2}$	15.1
445.55	$9^2G_{7/2,9/2} - 5^2F_{7/2}$	18.0	664.67	----------	----

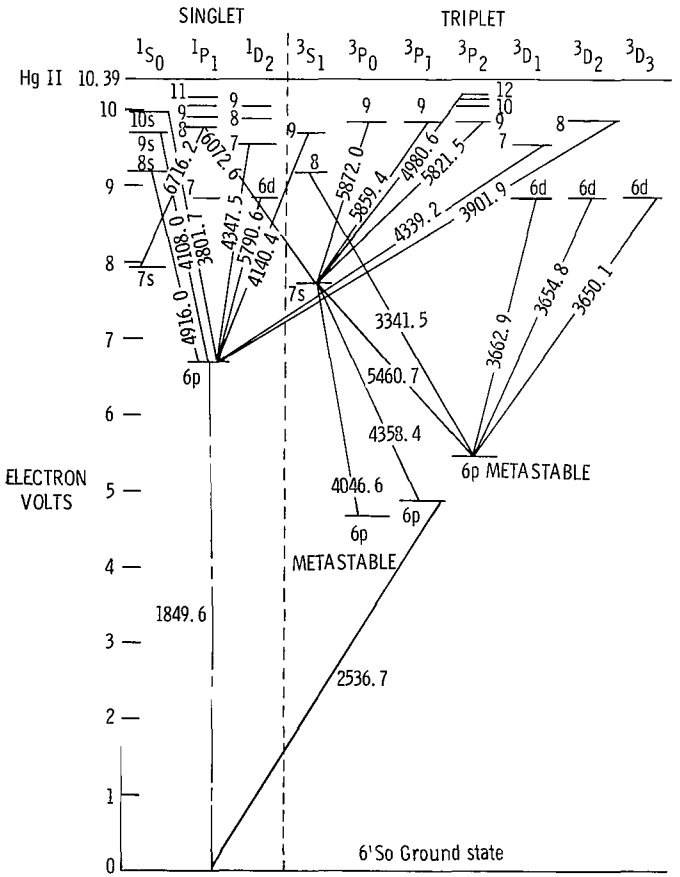

Figure 6. - Energy level diagram for Hg I.

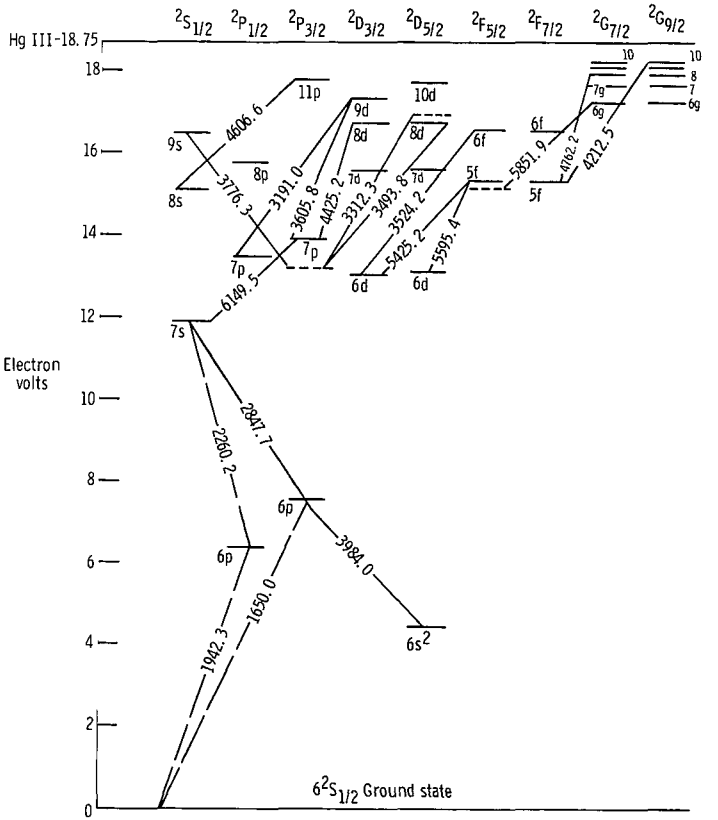

Figure 7. - Energy level diagram for Hg II.

The two electrons in the outer shell give the atom a helium-like structure. That is, the atomic levels consist of singlet and triplet series. Because of the larger atomic number for mercury, however, the radiation spectrum is more complicated than that of helium. This complication arises from the appreciable splitting of the triplet levels and from the allowed singlet-triplet transitions in mercury.

The energy level diagram of figure 6 includes the significant levels observed in this study. This diagram was constructed from the data of table I with the aid of reference 12. With the exception of the 185-nanometer resonant transition (broken line), the transitions given in the figure are representative of those observed and recorded in table I. The 185-nanometer line was not observed because transitions at wavelengths less than 230 nanometers were not within the range of the optical detection system.

Because the Hg II ion has only one electron in the outer shell it has a doublet structure for the excited states. All the ion levels observed in this study are given in figure 7. Levels for which the electronic configurations were unknown are represented by horizontal dashed lines. The transitions (shown by long-dash lines) were not observed but are presented for completeness. The lowest excited state of Hg II is a $6^2D_{5/2}$ metastable level with an energy of 4.5 electron volts above the ground state.

In addition to singly charged mercury ion excitation, excitation of doubly charged ions (Hg III) was also observed. Excitation of Hg III was detected most strongly at 479.7 nanometers. The upper level for this transition is located at 15.6 electron volts above the ground state for the doubly charged ion. With long exposure times, other weak Hg III excitations were observed at 331.2 nanometers at the upper state energy of 16.5 electron volts, 421.67 nanometers, at 15.0 electron volts, 355.7 nanometers at 16.5 electron volts, and 521.0 nanometers at 15.2 electron volts. Examination of the 1.5-meter-diameter thruster spectrum also revealed a very weak excitation at 396.8 nanometers, which Schaffernicht (ref. 15) has identified as Hg IV.

Impurities observed in the discharge are tabulated in table III. In general, only the most persistent lines of the particular element were observed. Only iron lines were observed in the 30-centimeter-diameter thruster, but barium, chromium, and iron were found as faint lines in the 1.5-meter-diameter thruster. The barium originated from the oxide cathodes used. Chromium and iron probably originated from the stainless steel thruster housing and anode in the 1.5-meter thruster. The iron in the 30-centimeter thruster could have originated from the thruster housing and anode or from the mild-steel hollow cathode pole piece. If the impurity source were mild steel, this might explain the absence of chromium in the spectrum of this thruster.

The present study indicated that the excitation of impurities in the discharge plasma was small. The total number and intensity contribution of the impurity lines to the radiation spectrum at the normal thruster operating discharge energy was substantially less than that of either the Hg I or Hg II contributions. This result suggests that the effect of these impurities on thruster performance was negligible.

TABLE III. - IMPURITIES IN 1.5-METER-DIAMETER THRUSTER

Wavelength, nm	Impurity	Wavelength, nm	Impurity
350.11	BaI	425.43	CrI
358.12	FeI	427.17	FeI
[a]371.99	FeI	427.48	CrI
[a]373.71	FeI	428.97	CrI
374.94	FeI	455.40	BaI
385.94	FeI	553.56	BaI
		614.17	BaI

[a]Also observed in 30-cm-diam thruster.

THRUSTER DIAGNOSTICS USING SPECTRAL LINE AMPLITUDES

Theory

The observed spectral amplitude is a measure of the emitted photons of energy corresponding to the wavelength of the spectral line. The problem is to relate the observed number of transitions at a given wavelength to the physical processes populating the energy level producing the photon emission (ref. 16). The following statements can be made on the physical nature of the discharge plasma within electron bombardment thrusters.

The discharge operates at low pressure (less than 10^{-3} torr) so that collisional broadening of spectral lines, collisional energy transfer between atoms, and three-body volume recombination would be expected to have a negligible effect on the observed line amplitudes (ref. 17). With exception of the resonant states, absorption should play a negligible role in excited state populations.

The ion chamber plasma, although essentially a steady-state discharge, was not in thermal equilibrium. This was shown by presuming that such equilibrium did exist in the discharge plasma and then applying equilibrium theory and the Boltzmann-Saha equations (refs. 18 and 19) to calculate electron temperatures from the observed line amplitude. Electron temperatures T_e were calculated that were one to two orders of magnitude below expected values based on Langmuir probe measurements. These low T_e values result from application of thermal equilibrium equations to nonequilibrium sustained plasmas (ref. 20).

Langmuir probe measurements of such discharges (refs. 2, 4, and 21) indicate that the electron distribution consists of nearly monoenergetic, or primary, electrons at an energy determined by the discharge chamber potential difference and a low-temperature

Maxwellian distribution. In order to interpret the observed spectral line amplitudes in terms of the electron energy producing the emitted radiation, it is necessary to incorporate a theoretical model of the discharge plasma. Because, in principle, both kinds of electrons can contribute to excitation and ionization of mercury atoms, a theoretical model of the discharge plasma should incorporate excitation and ionization by both groups.

With these preliminary considerations, the rate of populating the j^{th} excited state due to collision excitation from the ground state is given by

$$\dot{N}_j = N_o \left[N_m S_j(T_e) + N_p S_j(E_p)\right] \text{ cm}^{-3} \text{ sec}^{-1} \tag{1}$$

where $S_j(T_e)$ is the Maxwell averaged excitation coefficient for the j^{th} state and $S_j(E_p)$ is the excitation coefficient averaged over the primary electron distribution. (All symbols are defined in appendix A.)

The number of $j \rightarrow k$ transitions is then given by the steady-state relation

$$N_{jk} = \dot{N}_j \overline{A}_{jk} \text{ cm}^{-3} \text{ sec}^{-1} \tag{2}$$

where $\overline{A}_{jk}$ is the relative transition probability for the $j \rightarrow k$ transition, $\overline{A}_{jk} = A_{jk}/A_{j,tot}$. Equation (2) can be rewritten with the aid of equation (1) such that

$$N_{jk} = N_o N_m \left[1 + \varphi X_{jk}(T_e, E_p)\right] S_{jk}(T_e) \tag{3}$$

where

$$\varphi = \frac{N_p}{N_m}$$

$$X_{jk}(T_e, E_p) = \frac{S_{jk}(E_p)}{S_{jk}(T_e)} \tag{5}$$

and

$$S_{jk} = \langle Q_{jk} V_e \rangle$$

where the brackets denote averaging over the appropriate electron distribution. The quantities Q_{jk} are related to the excitation cross sections Q_j by the relation

$$Q_{jk} = Q_j \overline{A}_{jk} \tag{6}$$

They are the optical excitation functions for producing the observed spectral line corresponding the the $j \rightarrow k$ transition. The most recent measurements of optical excitation cross sections for mercury are those of Anderson, Lee, and Lin (ref. 22). A complete compilation of available mercury atom optical excitation functions can be found in reference 23.

In order to obtain the electron temperature and primary electron fraction, it was necessary to form a ratio of two line amplitudes. Examination of the observed mercury spectrum resulted in the selection of spectral lines at 365 nanometers (3650 Å) (6^3D_3 - 6^3P_2) and 365.5 nanometers (3655 Å) (6^3D_2 - 6^3P_2). Population of the 6^3D_3 level from higher lying states by cascading is negligible in the electron-energy range of interest (ref. 22), and there is no singlet mixing of this state. The 6^3D_2, however, mixes strongly with the 6^1D_2 to produce an optical excitation characteristic of the singlet state (ref. 22). These optical excitation functions are shown in figure 8. The calculated 365.0-nanometer excitation cross section using Gryzinski's theory (refs. 24 and 25) is also given for purposes of comparison. The excitation cross sections for these two lines are thus sufficiently different in their dependence on electron energy that the line ratios vary significantly. Thus, the method described in references 20 and 26 can be used to obtain electron temperature and primary electron fraction.

From equation (3) the ratio of the number of 365.5-nanometer transitions to 365.0-nanometer transitions (the ratio of spectral line amplitudes) is given by

$$\frac{N_{365.5}}{N_{365.0}} = \left[\frac{1 + \varphi X_{365.5}(T_e, E_p)}{1 + \varphi X_{365.0}(T_e, E_p)}\right] \frac{S_{365.5}(T_e)}{S_{365.0}(T_e)} \tag{7}$$

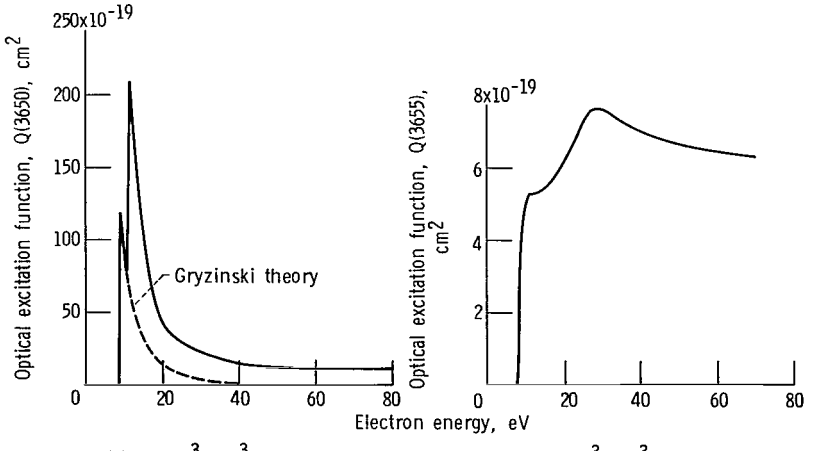

(a) For 6^3D_3-6^3P_2 transition. (b) For 6^3D_2-6^3P_2 transition.

Figure 8. - Optical excitation functions for HgI (refs. 24 and 25).

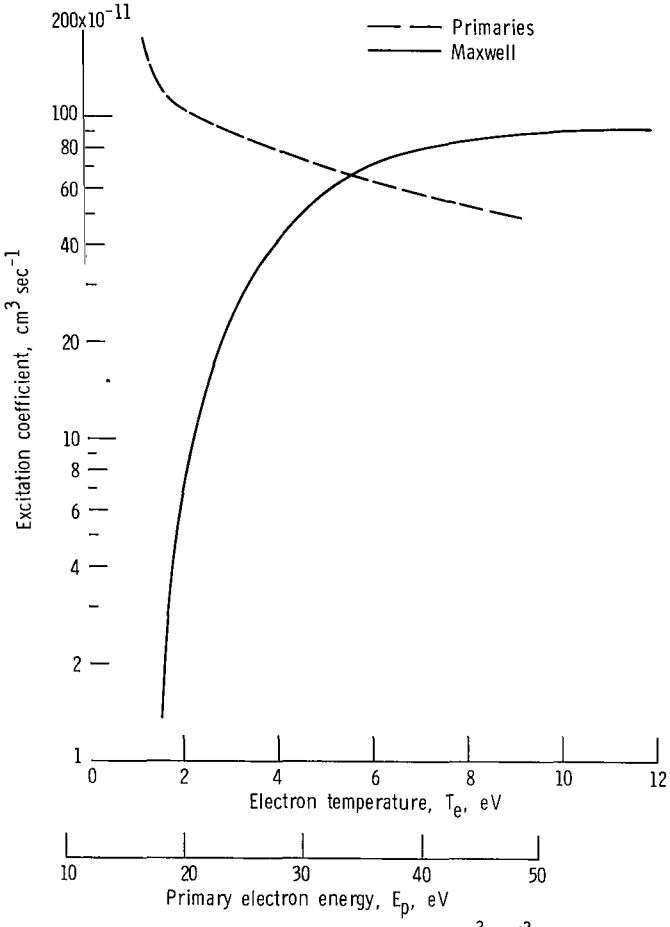

Figure 9. - Excitation coefficients for the 6^3D_3-6^3P_2 transition of HgI at 365.0 nanometers.

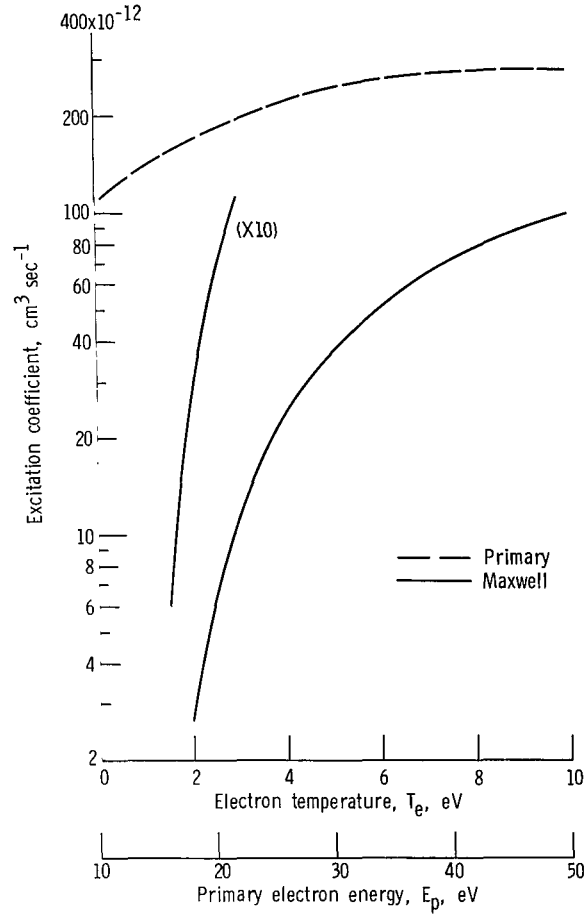

Figure 10. - Excitation coefficients for the 6^3D_2-6^3P_2 transition of HgI at 365.5 nanometers.

The variations of the appropriate excitation coefficients with electron temperature or primary electron energy are given in figures 9 and 10.

In order to use equation (7) to obtain primary electron fractions φ and electron temperatures T_e, it was necessary to choose a value for the primary electron energy E_p. Previous studies of the discharge of such thrusters (ref. 27) indicated that the primary electron energy can be related to the discharge chamber potential difference by the expression

$$E_p = \Delta V_I - V_P \tag{8}$$

where V_P is the plasma potential in the cathode-magnetic pole piece region. In the present study this potential V_P was taken to be 16 volts, based on electric probe measurements reported in reference 27.

A qualitative estimate of the sensitivity of the transition number ratio $N_{365.5}/N_{365.0}$ to primary electron energy is shown in figure 11. Here, the left side of equation (7) was plotted against E_p at two electron temperatures and three values of

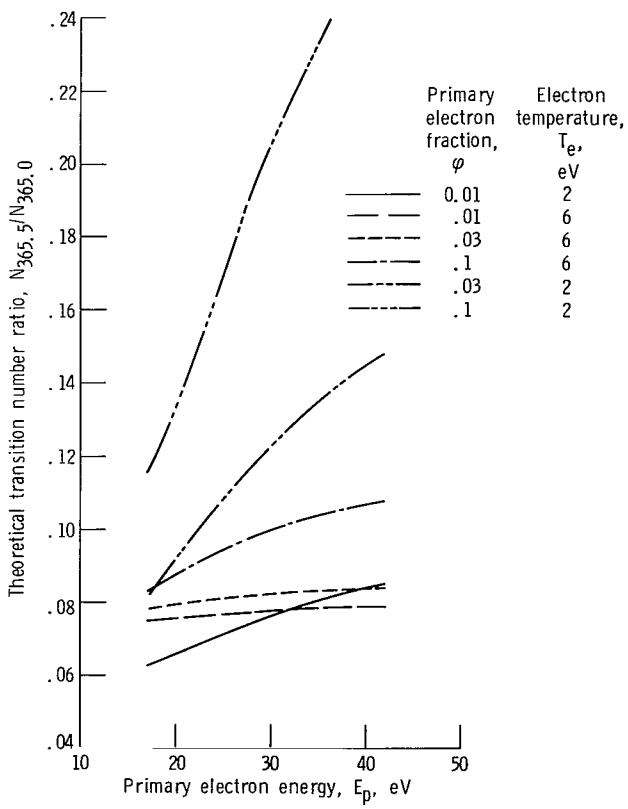

Figure 11. - Theoretical transition number ratio against primary electron energy.

primary fraction. It was evident from such plots that the transition number ratio became less sensitive to changes in primary energy as the electron temperature was increased. Thus, an error in the selection of E_p would have the largest effect at the lower electron temperatures and high primary fraction.

Atom Excitation

The preceding theory was used to interpret the results of spectroscopic measurements obtained on a 30-centimeter-diameter hollow cathode bombardment thruster. Spectral line amplitudes were obtained for discharge chamber potential differences ΔV_I of 33, 38, 43, and 58 volts. The discharge current was maintained at 8 amperes, and the thruster beam current was constant at 1.5 amperes. At each discharge voltage the ratio of the number of 365.5- to 365.0-nanometer transitions was calculated at four radial positions. These ratios are shown graphically in figure 12. Here the measured ratio $N_{365.5}/N_{365.0}$ is plotted at the four radial positions. Of particular interest is the minimum occurring at 22 electron volts at all radial positions except that furthest from the thruster axis. Such a minimum can be explained by the existence of nonrandomized primary electrons in the plasma discharge with the aid of figure 13 (see appendix B).

The results of the analysis are summarized in figure 14. Here, the variation in the range of electron temperature with primary electron energy is presented for four radial positions. The boundaries of the crosshatched regions were determined by the range of

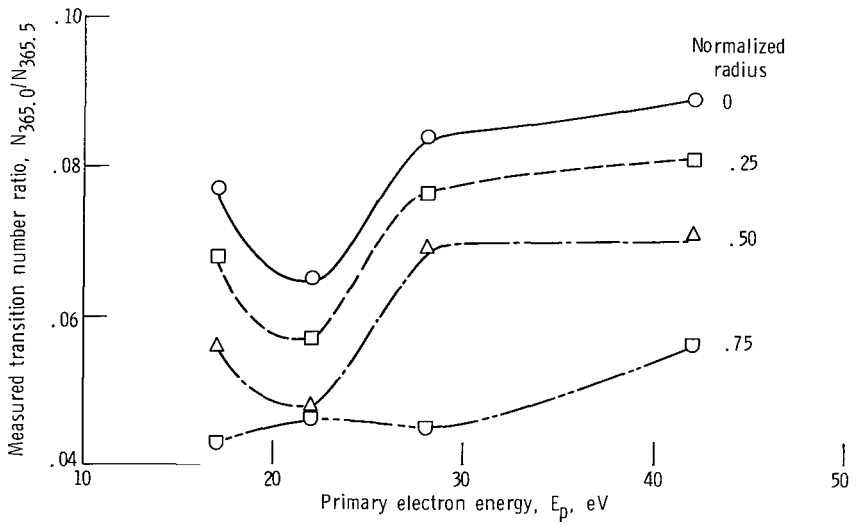

Figure 12. - Measured transition number ratio against primary electron energy, where $E_p = \Delta V_I - 16$ eV.

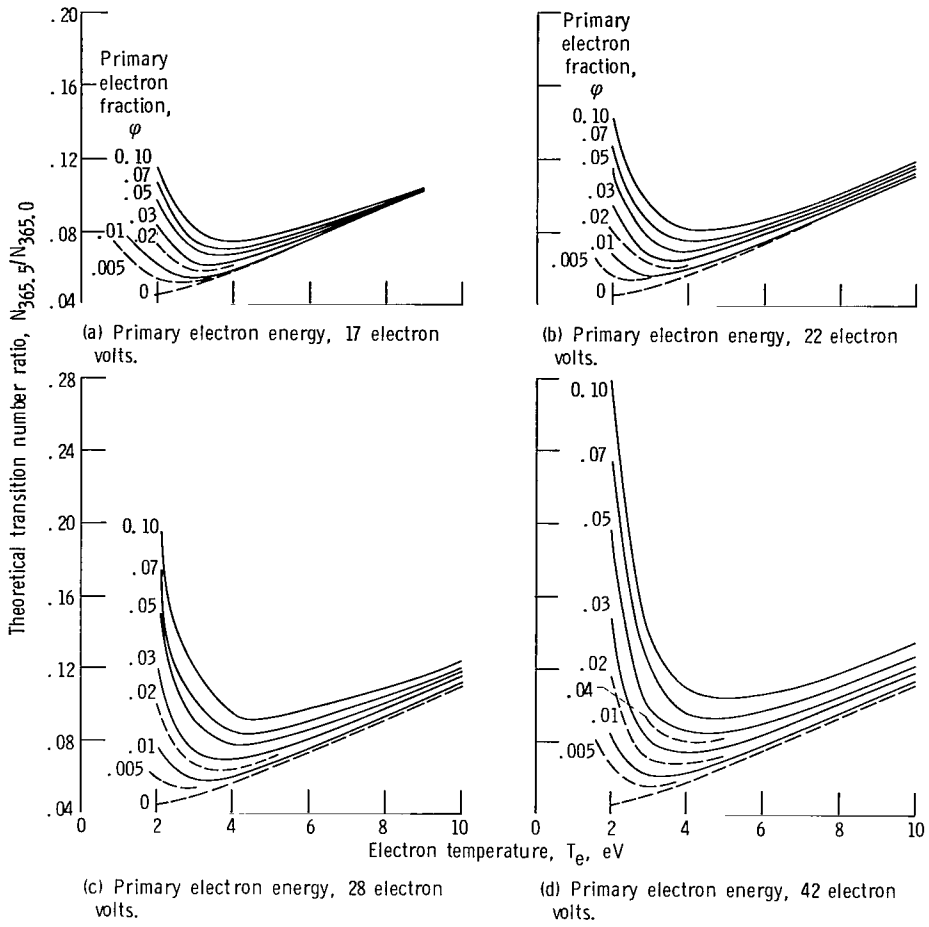

Figure 13. - Theoretical transition number ratio against electron temperature.

primary electron fraction. The values of electron temperature obtained were in general agreement with Langmuir probe measurements of hollow cathode thruster discharges (ref. 4). The result that the largest values of primary electron fraction and electron temperature were obtained on the thruster axis, whereas the smallest values of these parameters were obtained at three-quarters radius, is consistent with recent measurements of a primary electron region centered about the thruster axis (ref. 28).

Effects of Metastables

For mercury the contribution to excited states by collisional excitation from metastable states can be shown to be less than the direct excitation from the ground state and could thus be neglected. The ratio between collisional excitation of the 6^3D_3 state from

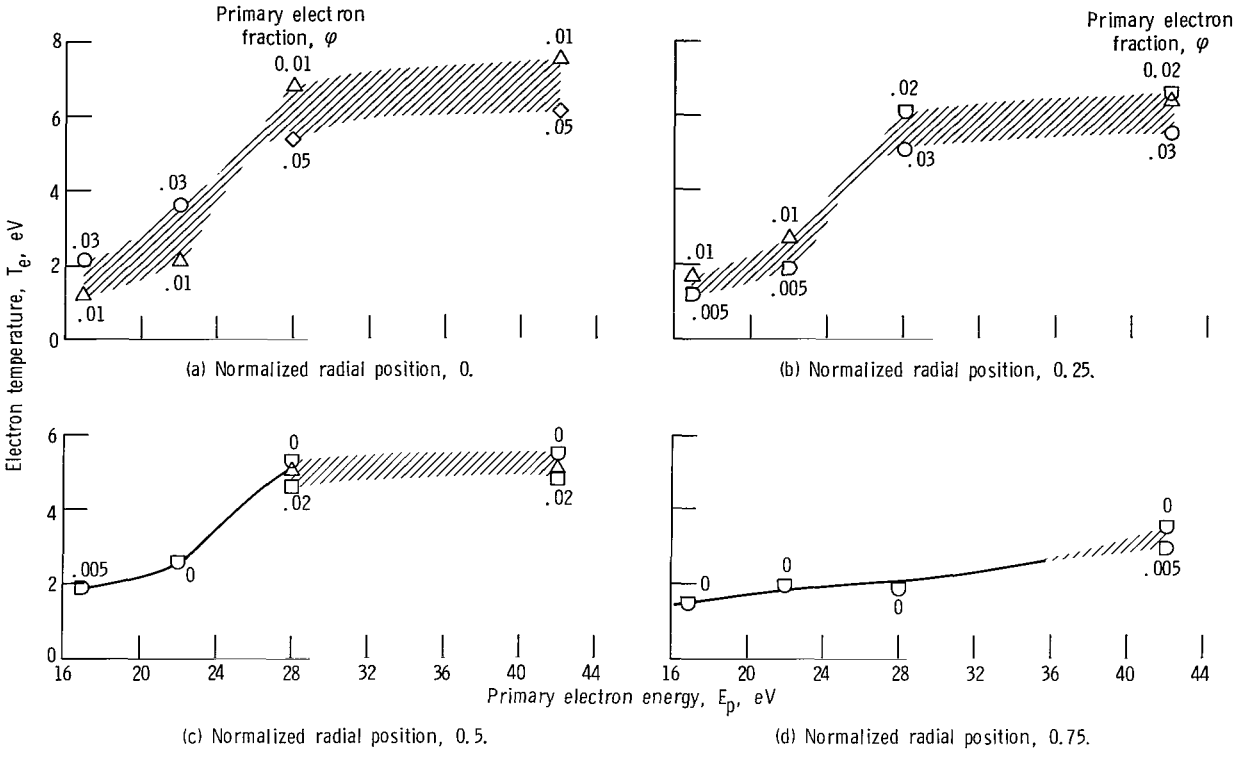

Figure 14. - Electron temperature against primary electron energy.

the 6^3P_0 metastable level to the rate of collisionally populating the 6^3D_3 from the ground state was calculated to be about 0.005 over an electron temperature range of 4 to 7 electron volts. The corresponding ratio for excitation from the 6^3P_2 metastable state was about 0.027 over the same electron temperature range. These ratios were even lower at electron temperatures below 4 electron volts. The calculations were based on the Gryzinski theory (refs. 24 and 25) and the assumption of a pure Maxwellian electron distribution. Experimentally, it was found that the primary electron density was generally less than 5 percent of the Maxwellian electron density. This fact, in conjunction with the fact that excitation coefficients for primary and Maxwellian electron excitation are of the same order of magnitude (figs. 9 and 10), implies that these estimates of the metastable level contribution to equation (1) are reasonable. Thus, exclusion of the metastable contribution to the collisional excitation of the 6^3C states was justified.

Ion Excitation

Table IV lists the electron energy required to produce various degrees of ionization

TABLE IV. - IONIZATION ENERGIES AND CROSS SECTIONS

FOR MERCURY (REFS. 12, 23, AND 28)

Ionization reaction	Minimum energy required, eV	Maximum cross section, cm^2
Hg I → Hg II	10.43	5.4×10^{-16}
Hg I → Hg III	29.2	5.4×10^{-17}
Hg I → Hg IV	63.4	3.0×10^{-18}
Hg II → Hg III	18.75	4.2×10^{-16}
Hg III → Hg IV	34.2	6.0×10^{-16}

of mercury by electron bombardment (ref. 12). Kupriyanov, and Latypov (ref. 29) have measured cross sections for the last two reactions of table IV, and several authors (ref. 23) have measured the cross section for production of multiply ionized mercury atoms. Optical excitation functions for mercury ions are essentially unavailable. In reference 29 the excitation function for the 284.7-nanometer line of Hg II is reported. Here, however, excitation was the result of electron - neutral-atom collisions rather than electron-ion collisions. In the present work, calculated excitation cross sections based on the Gryzinski semiclassical method were used to obtain mercury ion excitation coefficients.

For ion excitation the spectral amplitude at 398.4 nanometers, corresponding to the $6^2P_{3/2}$ - $6s^2\ ^2D_{5/2}$ transition in Hg II (see fig. 7), was used as the diagnostic line. It has been estimated (ref. 30) that contributions from cascading to the population of the $6^2P_{3/2}$ level should be less than 10 percent. This line produced the strongest signal in the observed Hg II excitation spectrum. The calculated excitation cross section for the $6^2P_{3/2}$ level is given in figure 15. Also shown is the calculated level excitation cross sections for the $5d^8_{5/2,\,3/2}\ 6s^2$(J=4) Hg III line at 479.7 nanometers. These cross sections are plotted as functions of electron energy. Excitation from the ground state of the ion (single ion for the 398.4-nm line and double ion for the 479.7-nm line) was assumed. From comparisons between such calculated cross sections for helium and experimentally measured helium optical excitation functions (ref. 25) the calculated cross sections for mercury are expected to be within an order of magnitude of actual cross sections.

The variation of the ion to neutral fraction was determined as a function of primary electron energy at different radial locations in a 30-centimeter hollow cathode thruster. Using the method to obtain equation (7) measured amplitudes at 398.4 nanometers for

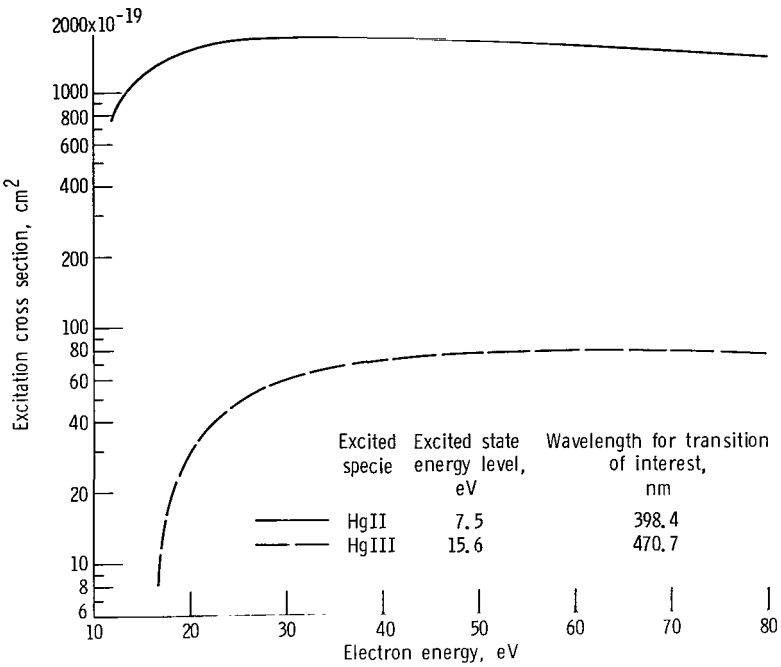

Figure 15. - Theoretical level excitation cross sections for HgII and HgIII.

Hg II and 365.0 nanometers for Hg I were ratioed to obtain the expression

$$\frac{N_+}{N_0}\overline{A}_{398.4} = \frac{N_{398.4}}{N_{365.0}} \frac{1 + \varphi X_{365.0}(E_p, T_e)}{1 + \varphi X_{398.4}(E_p, T_e)} \frac{S_{365.0}(T_e)}{S_{398.4}(T_e)} \tag{9}$$

The quantity $\overline{A}_{398.4}$ is the relative transition probability. Its value is unknown, but is expected to be substantially less than one. This is because the $6^2P_{3/2}$ upper state of the 398.4-nanometer transition is a resonant state and thus would most probably radiate to the ground state. The excitation coefficient coefficient ratios $X_\lambda(E_p, T_e)$ have been defined earlier and can be obtained from figure 16. Because $\overline{A}_{398.4}$ is constant, the right side of equation (9) yields the relative variation of N_+/N_o. The range of values of φ and T_e used were obtained from figure 14. The relative variation of N_+/N_o is given in table V (third column) as a function of E_p and radius. The calculations indicate that the ion fraction N_+/N_o did not vary appreciably with discharge voltage.

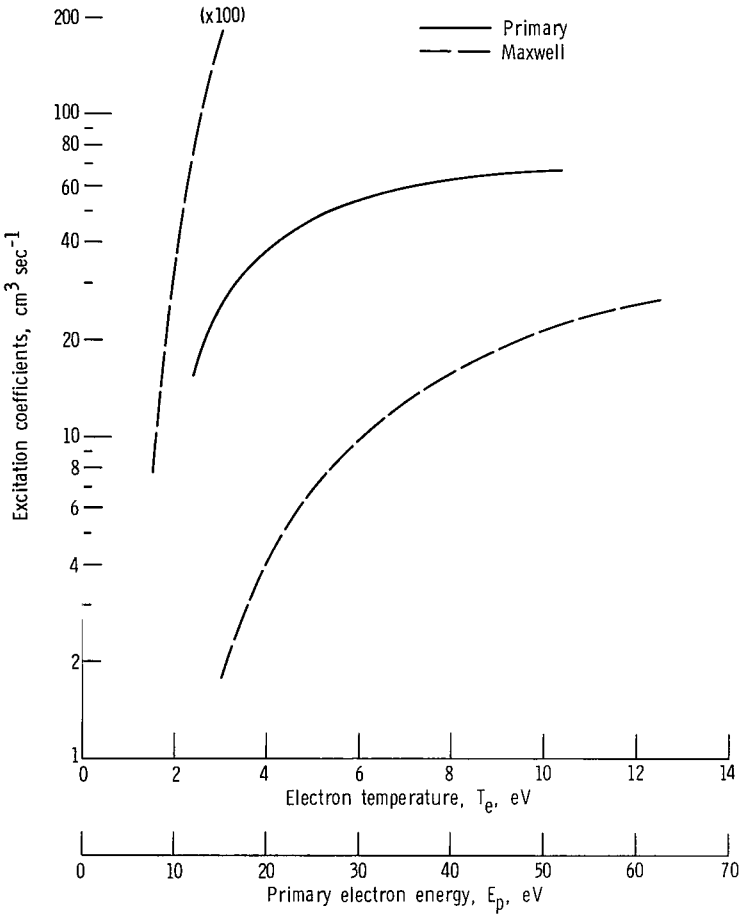

Figure 16. - Excitation coefficients for the $6^2P_{3/2}$ level of HgII. Transition at 398.4 nanometers.

TABLE V. - CALCULATED ION FRACTIONS

Radial location, normalized	Primary electron energy, eV	Density ratios	
		$N_+/N_o\ \overline{A}(3984)$ $(\times 10^{+4})$	N_{++}/N_o
0	17	5.5 - 8.8	<0.009
	22	7.6 - 10.5	0.005 - 0.007
	28	7.8 - 8.2	0.008
	42	7.2 - 7.4	0.020 - 0.022
0.25	17	4.5 - 7.2	<0.004
	22	10.4 - 12.0	0.006 - 0.007
	28	5.4	0.006
	42	6.9 - 8.3	.019
0.50	17	7.3	<0.004
	22	8.3	.004
	28	4.4 - 5.9	.004
	42	6.2 - 6.3	.013
0.75	17	7.7	<0.004
	22	7.0	<.004
	28	8.3	<.004
	42	4.2 - 4.4	<.004

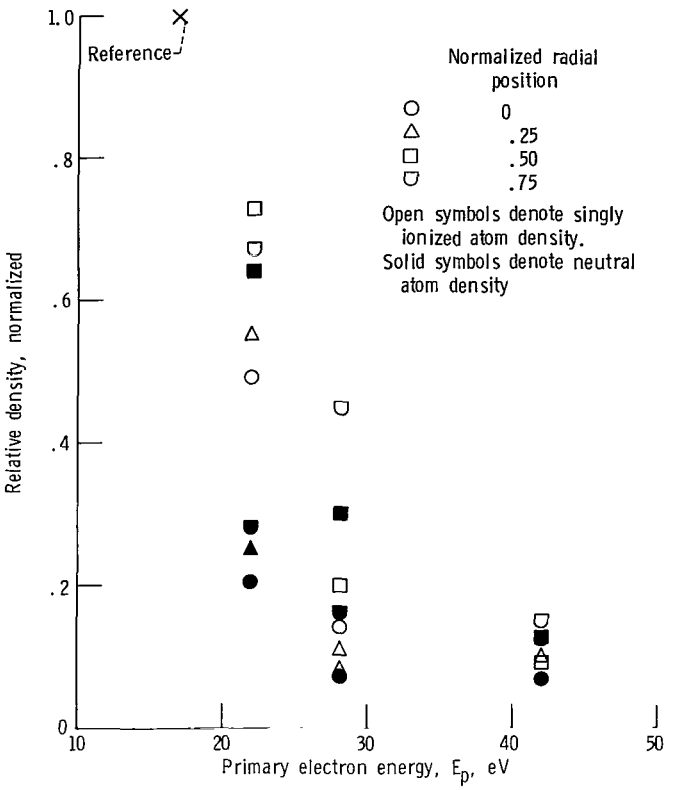

Figure 17. - Normalized ion and atom density variations with electron energy. 30-Centimeter-diameter hollow-cathode thruster; ion beam current, 1.5 amperes.

The relative variation of N_+ can be obtained from the relation

$$N_+ \propto \left\{ \frac{N_{398.4}}{\left[1 + \varphi X_{398.4}(E_p, T_e)\right] S_{398.4}(T_e)} \right\}^{1/2} \tag{10}$$

where it is assumed that $N_+ \sim N_m$. Combining equations (10) and (9) enables us to obtain the relative variation of N_0. These variations are shown in figure 17, in which an average of the normalized ion and neutral atom densities are plotted as functions of primary electron energy. Maximum densities occurred at the lowest energy (17 eV), and all the data were normalized to unity at this energy. The marked decrease in both ion and atom densities can probably be attributed to the decrease in propellant flow required to maintain the constant beam current (1.5 A) with increased discharge chamber potential difference. This fact suggests the possibility of relating propellant flow changes to changes in atom and ion spectral amplitudes. Further studies at varying thruster operating conditions would be required, however, to determine whether spec-

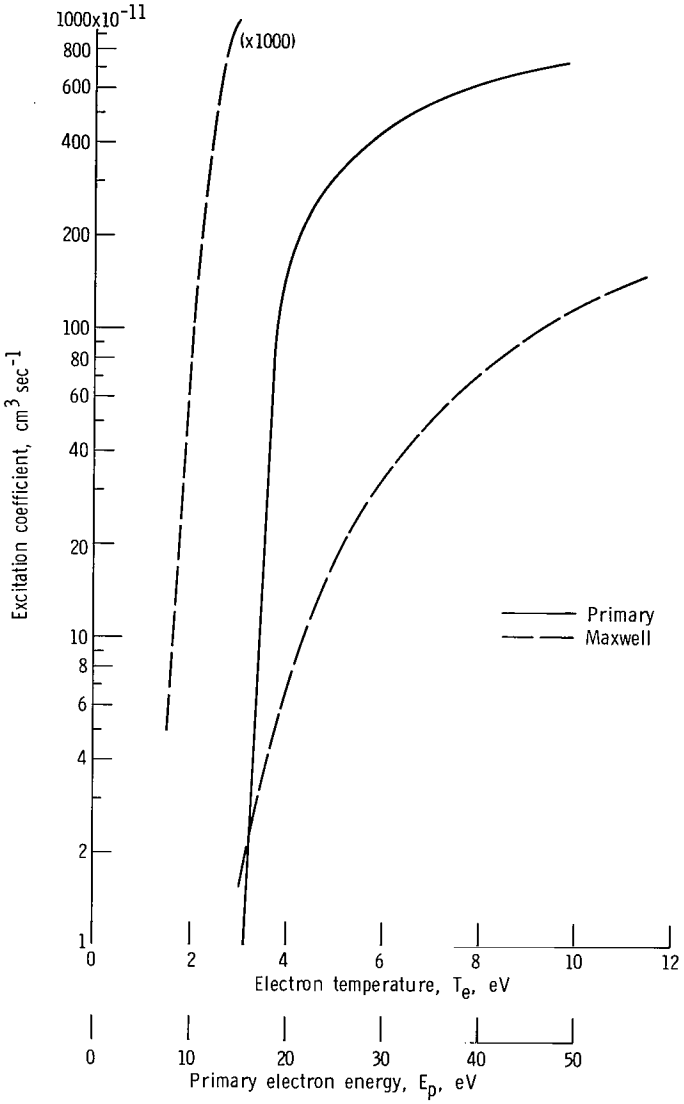

Figure 18. - Excitation coefficients for the $5d^8_{5/2,3/2}6s^2(J = 4)$ level of HgIII. Transition at 479.7 nanometers.

troscopic techniques could be used to monitor propellant flow variations.

Excitation of doubly charged mercury ions at 479.7 nanometers were also measured in the 30-centimeter-diameter thruster. An expression analogous to equation (9) (with 479.7 nm substituted for 398.4 nm) can be used to obtain N_{++}/N_o. The appropriate excitation coefficients are given in figure 18. In this case, $\overline{A}_{479.7} = 1$, because the upper state of this transition has only a single path for radiative decay (ref. 31). Thus the spectral amplitude ratio gives the fraction of N_{++} in the discharge directly. These fractions are given in the last column of table V. The accuracy of these measurements depends markedly on the accuracy of the excitation coefficients used. Because, to the authors' knowledge, no measured excitation functions for Hg III are available, it is impossible at present to assess the accuracy of these calculations. However, the N_{++}/N_o ratios of table V were found to be consistent with measurements of double ion currents obtained in the ion beam exhaust (ref. 32).

It should be noted that excitation of Hg III at an electron energy of 17 electron volts was observed at all radial positions, although quite weakly. The existence of Hg III at such low electron energies is to be expected because the threshold for ionizing Hg II to Hg III from the $6^2D_{5/2}$ metastable level of Hg II is about 15 electron volts. In addition, the "tail" of the low-temperature Maxwellian distribution of electrons can produce both ionization of Hg II and excitation of Hg III.

A POSSIBLE MEASUREMENT OF NEUTRALIZER-BEAM COUPLING VOLTAGE

The orthogonal slit arrangement (fig. 5) was used to obtain the $N_{365.5}/N_{365.0}$ ratio in the region of the neutralizer. The results are shown in figure 19. The center of the discharge chamber was located at $r = 0$. The $N_{365.5}/N_{365.0}$ transition ratio in the neutralizer region was of the order of 0.14 to 0.18. These values were substantially greater than those obtained from the discharge region (fig. 12). Using the primary plus Maxwellian electron energy distribution theory described by figure 13, such high values suggest a large primary electron concentration and a very low electron temperature (of the order of 1 eV). Hence, excitation by Maxwellian electrons can be neglected. A primary electron energy in the neutralizer region of about 20 to 22 electron volts was thus obtained. This result is in good agreement with potential probe measurements of the neutralizer-beam coupling voltage for neutralizers operating in spot mode (ref. 33). The $N_{365.5}/N_{365.0}$ ratio dropped off rapidly toward the thruster side of the neutralizer, suggesting randomization of neutralizer electrons. The intensity ratios in the neutralizer region appeared to be relatively insensitive to varying thruster parameters at a constant beam current of 1.5 amperes.

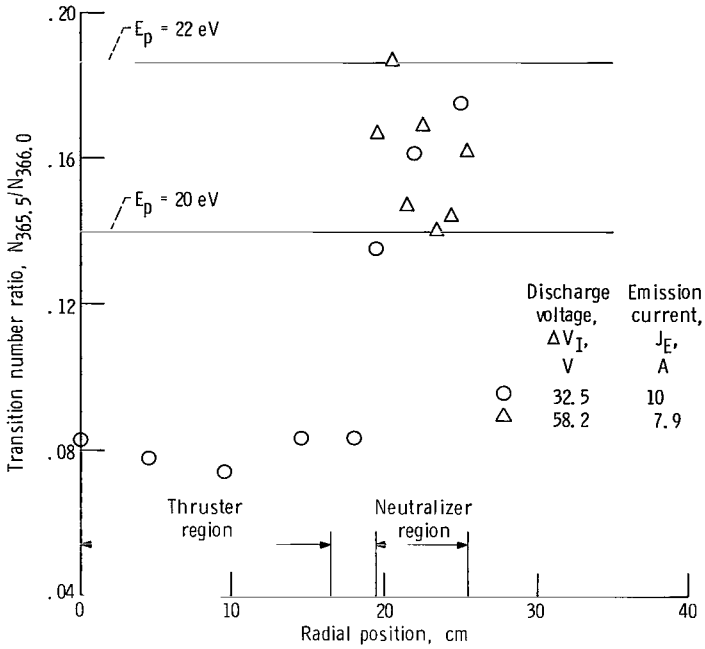

Figure 19. - Measurement of neutralizer transition number ratio for 30-centimeter-diameter thruster. Ion beam current, 1.5 amperes.

TABLE VI. - TRANSITIONS FROM THE 7^3S_1 LEVEL IN MERCURY

Wavelength, nm	Transition
404.7	$7^3S_1 - 6^3P_0$
435.8	$7^3S_1 - 6^3P_1$
546.1	$7^3S_1 - 6^3P_2$

RELATIVE AMPLITUDES OF THE $7^3S_1 - 6^3P_{0,1,2}$ TRANSITIONS

Table VI lists the wavelengths of the so-called visible triplet of the mercury spectrum. Because these transitions originate from the same state (7^3S_1), the relative spectral line amplitudes are independent of the level excitation cross section. The transition ratios $N_{404.7}:N_{435.8}:N_{546.1}$ are thus a direct measure of the relative transition probabilities for these lines. Several authors have reported measured values for these ratios, most of which have been tabulated in reference 34. In table VII, this tabulation is repeated, including the measurements of Anderson (ref. 22) and the present authors. In reference 22 the transition probabilities were calculated to obtain the theoretical values for these ratios given in the table.

The results of the present work were based on seven measurements made along different radial locations in the 30-centimeter-diameter hollow-cathode thrusters. The resulting relative transition probabilities are seen to be in general agreement with previous work and in good agreement with the reported theoretical values. This fact provides additional verification of the measurements obtained in this study.

TABLE VII. - RELATIVE TRANSITION RATIOS

FOR THE VISIBLE TRIPLET IN Hg

Source	4047	4358	5461
Hanle and Schaffernicht (ref. 35)	47	100	82
Theime (ref. 36)	43	100	77
Lebedeva and Fabrikant (ref. 37)	43	100	86
Schouten (ref. 38)	37	100	134
Jongerius (ref. 39)	37	100	125
Frisch and Klucharyov (ref. 34)	37	100	116
Anderson, et al. (ref. 22):			
Theory	46	100	70
Experiment	36±3	100	96±13
Present work	38±4	100	71±14

CONCLUDING REMARKS

The excitation spectrum of mercury atoms and ions produced by electron bombardment thrusters has been determined. The discrete spectrum has been categorized for wavelengths between 230 and 700 nanometers (2300 and 7000 Å). Excitation of singly, doubly, and possibly triply ionized mercury has been detected.

Spectral line amplitude measurements indicated that the discharge was a nonequilibrium, sustained plasma. The energy distribution of electrons in the discharge of hollow-cathode thrusters can be represented by a distribution of monoenergetic electrons superimposed on a Maxwellian electron distribution. Ratios of the spectral line amplitudes at 365.5 and 365.0 nanometers (3655 and 3650 Å) were formed to obtain electron temperatures and ratios of primary to Maxwellian electron densities at four primary electron energies and different radial locations. It was found that the electron temperature ranged from about 1.2 to 7.5 electron volts and that the primary to Maxwellian electron density ratio ranged from zero to about 0.05. These values depended on primary electron energy and radial location in the thruster.

Normalized ion and neutral densities decreased with increasing discharge voltage at constant emission current and beam current. It was presumed that this behavior was attributable to a decreasing propellant flow with increasing voltage. This decrease in flow was required in order to maintain a constant beam current. Spectroscopic measurements in the region of the neutralizer operating in spot mode indicated a coupling voltage of the order of 20 to 22 volts.

The fraction of doubly charged mercury ions did not exceed about 2 percent of the atom density in the discharge plasma at a discharge voltage of 58 volts. At lower discharge voltages this fraction did not exceed about 0.8 percent.

One of the primary purposes of this investigation was to determine the extent to

which the optical radiation of electron bombardment thrusters could be used to study the discharges of such thrusters. The high sensitivity of the radiation output to changes in thruster parameters suggests potential engineering applications. For example, it may be possible to use the light output from the neutralizer region to control the neutralizer gas flow. It was concluded that this study demonstrated the applicability of spectroscopy as a diagnostic tool for thruster investigations.

Lewis Research Center,
National Aeronautics and Space Administration,
Cleveland, Ohio, August 19, 1971,
113-26.

APPENDIX A

SYMBOLS

A_{jk}	transition probability for $j \rightarrow k$ transition, sec^{-1}
$A_{j,tot}$	total transition probability for state j, sec^{-1}
$\overline{A}_{jk}$	relative transition probability, $A_{jk}/A_{j,tot}$
A_λ	relative transition probability at wavelength λ
D	atom orbital angular momentum, equal to 2
d	electron orbital angular momentum, equal to 2
E_p	primary electron energy (eq. (8)), eV
f	electron orbital angular momentum, equal to 3
Hg I, II, III	mercury atom, single ion and double ion, respectively
J	total atom angular momentum
J_B	ion beam current
N_j	rate of collisionally populating j^{th} state from the ground state
N_{jk}	number of $j \rightarrow k$ transitions, $cm^{-3}\ sec^{-1}$
N_m	Maxwell electron density, cm^{-3}
N_o	neutral atom density, cm^{-3}
N_p	primary electron density, cm^{-3}
N_λ	number of transitions at wavelength λ (spectral line amplitudes)
$N_{+,++}$	density of singly (and doubly) ionized atoms, cm^{-3}
P	atom orbital angular momentum, equal to 1
p	electron orbital angular momentum, equal to 1
Q_j	excitation cross section, cm^2
Q_{jk}	optical excitation function for $j \rightarrow k$ transition, m^2
r	radial position relative to thruster axis
S	atom orbital angular momentum, equal to 0
s	electron orbital angular momentum, equal to 0
$S_j(E_p)$	primary electron excitation coefficient at energy E_p to state j, $cm^3\ sec^{-1}$
$S_j(T_e)$	Maxwell electron excitation coefficient at temperature T_e to state j, $cm^3\ sec^{-1}$
S_{jk}	optical excitation coefficient for $j \rightarrow k$ transition
S_λ	excitation coefficient at wavelength λ
T_e	electron temperature, eV

V_p cathode-pole piece plasma potential, v

ΔV_I discharge chamber potential difference, v

v_e electron speed, cm sec^{-1}

$X_{jk}(E_p, T_e)$ optical excitation coefficient ratio, $S_{jk}(E_p)/S_{jk}(T_e)$

$X_\lambda(E_p, T_e)$ excitation coefficient ratio at wavelength λ

φ primary electron fraction, N_p/N_m

APPENDIX B

METHOD FOR INTERPRETING THE OBSERVED ATOM EXCITATIONS

In figure 13, equation (7) is plotted against electron temperature for the four primary electron energies studied. Several curves corresponding to different values of primary electron fraction φ, ranging from 0 to 0.1 are presented. It should be noted that curves of $\varphi > 0$ show a minimum. The intersection of the measured $N_{365.5}/N_{365.0}$ ratio with these theoretical curves was used to obtain the ranges of electron temperature and primary electron fraction corresponding to a given value of primary electron energy E_p, making use of the following assumptions:

(1) Increasing the primary electron energy increased the available discharge power per atom and hence increased the electron temperature. Thus the electron temperature obtained from figure 13(d) would be greater than the temperature obtained from figure 13(a).

(2) Because an increase in primary electron energy increased the mean relaxation time for primary electrons, it was assumed that the primary electron fraction did not decrease with increasing primary electron energy. The average primary fraction obtained from figure 13(d) would thus be greater than the average fraction obtained from figure 13(a).

(3) For values of primary electron energy E_p less than 22 electron volts, the measured $N_{365.5}/N_{365.0}$ ratio decreased with increasing electron energy. Also, the theoretical $N_{365.5}/N_{365.0}$ ratios of figure 13 decreased with increasing electron temperature for temperatures below about 4 electron volts. Thus, for $E_p \leq 22$ electron volts, points of intersection of the measured $N_{365.5}/N_{365.0}$ line to the right of the minimum of the theoretical curves of figure 13 were neglected. Similarly, for $E_p > 22$ electron volts, only points of intersection to the right of the minima were retained.

The allowable range of values for primary electron fraction at different radial locations was obtained using condition (2) and the following considerations. At a given radial location (e.g., $r = 0$) and primary electron energy equal to 22 electron volts, the measured $N_{365.5}/N_{365.0}$ ratio (equal to 0.065 at $r = 0$) was drawn tangent to the minimum of a particular φ-curve of figure 13(b). (For $r = 0$, the measured ratio at 0.065 was tangent to the primary electron fraction, $\varphi = 0.03$ curve at its minimum.) The resulting value of φ was the upper bound of the φ (and thus T_e) range associated with $E_p = 17$ and 22 electron volts. The lower bound was obtained from the intersection of the measured $N_{365.5}/N_{365.0}$ ratio at $E_p = 17$ electron volts with portions of the φ-curves of figure 13(a) to the left of the minima and from the fact that electron temperature was presumed to exceed about 1 electron volt at all thruster conditions. This assumption was based on the fact that temperatures lower than 1 electron volt charac-

terize a thermal equilibrium plasma. From our earlier discussion, it was argued that the discharge chamber plasma was not in thermal equilibrium. Thus, for the radial position $r = 0$, where $N_{365.5}/N_{365.0} = 0.074$ at $E_p = 17$ electron volts, the lower bound on the primary electron fraction φ (from fig. 13(a)) was about 0.01.

For $E_p > 22$ electron volts, the procedure used to obtain the appropriate ranges of electron temperature and primary electron fraction was as follows: The maximum primary electron fraction was obtained from the intersection of the measured $N_{365.5}/N_{365.0}$ ratio with the curves of figure 13(d). For the radial position $r = 0$, the largest value of φ intersected by $N_{365.5}/N_{365.0}$ equal to 0.089 was about 0.05. Thus, for primary energies less than 42 electron volts, intersection of measured $N_{365.5}/N_{365.0}$ values with curves of $\varphi > 0.05$ were disregarded, in accordance with condition (2).

The minimum value of φ for $E_p > 22$ electron volts was the same as the minimum φ value for $E_p < 22$ electron volts, again, in accordance with condition (2). Thus, for $r = 0$ and $E_p > 22$ electron volts, the range of φ was found to be $0.01 \leq \varphi \lesssim 0.05$. For $E_p \leq 22$ electron volts, the range was $0.01 \leq \varphi \leq 0.03$. Using the φ ranges and the appropriate curves of figure 13, the range of electron temperature for different values of E_p could be determined.

REFERENCES

1. Milder, Nelson L.: A Survey and Evaluation of Research on the Discharge Chamber Plasma of Kaufman Thrusters. J. Spacecraft Rockets, vol. 7, no. 6, June 1970, pp. 641-649.

2. Masek, T. D.: Plasma Properties and Performance of Mercury Ion Thrusters. Paper 69-256, AIAA, Mar. 1969.

3. Masek, T. D.: Plasma Characteristics of the Electron Bombardment Ion Engine. Rep. TR-32-1271, Jet Propulsion Lab., California Inst. Tech. (NASA CR-94554), Apr. 15, 1968.

4. Knauer, W.; Poeschel, R. L.; King, H. J.; and Ward, J. W.: Discharge Chamber Studies for Mercury Bombardment Ion Thrusters. Hughes Research Lab. (NASA CR-72440), Sept. 1968.

5. Milder, Nelson L.; and Sovey, James S.: Preliminary Results of Spectrographic Analyses of Kaufman Thrusters. Paper 70-176, AIAA, Jan. 1970.

6. Bechtel, Robert T.: Performance and Control of a 30-Centimeter Diameter, Low-Impulse Kaufman Thruster. Paper 69-238, AIAA, Mar. 1969.

7. King, H. J.; and Poeschel, R. L.: Low Specific Impulse Ion Engine. Hughes Research Lab. (NASA CR-72677), Feb. 1970.

8. Nakanishi, S.; and Pawlik, E. V.: Experimental Investigation of a 1.5-m-diam Kaufman Thruster. J. Spacecraft Rockets, vol. 5, no. 7, July 1968, pp. 801-807.

9. Finke, Robert C.; Holmes, Arthur D.; and Keller, Thomas A.: Space Environment Facility for Electron Propulsion Systems Research. NASA TN D-2774, 1965.

10. Harrison, George R., ed.: Tables of Wavelengths. MIT Press, 1939.

11. Paschen, F.: First Spark Spectrum of Mercury, Hg II. Preuss. Akad. Wiss. Berlin, Ber., no. 32, 1928, pp. 536-546.

12. Moore, Charlotte E.: Atomic Energy Levels as Derived from the Analyses of Optical Spectra. Vol. III. Circ. 467, National Bureau of Standards, 1958.

13. Mrozowski, S.: On the Spectra of Hg II and Hg III. Phys. Rev., vol. 61, nos. 9-10, May 1-15, 1942, pp. 605-613.

14. McLennan, J. C.; McLay, A. B.; and Crawford, M. F.: Spark Spectrum of Mercury, Hg II. Proc. Roy. Soc. (London), Ser. A, vol. 134, no. 823, Nov. 3, 1931, pp. 41-47.

15. Schaffernicht, W.: Optical Excitation Functions of Mercury Lines. Ziet. f. Physik, vol. 62, no. 1-2, 1930, pp. 106-142.

16. St. John, Robert M.; Miller, Frank L.; and Lin, Chun C.: Absolute Electron Excitation Cross Sections of Helium. Phys. Rev., vol. 134, no. 4A, May 18, 1964, pp. 888-897.

17. Moiseiwitsch, B. L.; and Smith, S. J.: Electron Impact Excitation of Atoms. Rev. Mod. Phys., vol. 40, no. 2, Apr. 1968, pp. 238-353.

18. Griem, Hans R.: Plasma Spectroscopy. McGraw-Hill Book Co., Inc., 1964.

19. McWhirter, R. W. P.: Spectral Intensities. Plasma Diagnostic Techniques. R. H. Huddlestone and S. L. Leonard, eds., Academic Press, 1965, pp. 201-264.

20. Sovie, R. J.: The Effects of Cascading and Metastable Atoms on the Determination of Electron Temperature from Relative Line Intensities in a Tenuous Helium Plasma. J. Quant. Spectrosc. Radia. Transfer, vol. 8, 1968, pp. 833-838.

21. Strickfaden, William B.; and Geiler, Kenneth L.: Probe Measurements of the Discharge in an Operating Electron Bombardment Engine. AIAA J., vol. 1, no. 8, Aug. 1963, pp. 1815-1823.

22. Anderson, Richard J.; Lee, Edward T. P.; and Lin, Chun C.: Electron Excitation Functions of Mercury. Phys. Rev., vol. 157, no. 1, May 5, 1967, pp. 31-40.

23. Kieffer, L. J.: Compilation of Low Energy Electron Collision Cross Section Data. Part I: Ionization, Dissociative Processes, and Vibrational and Rotational Excitation. Rep. JILA-6, pt. 1, Univ. of Colorado, Jan. 10, 1969.

24. Gryziński, Michal: Classical Theory of Atomic Collisions. I. Theory of Inelastic Collisions. Phys. Rev., vol. 138, no. 2A, Apr. 19, 1965, pp. 336-358.

25. Dugan, John V., Jr.; and Sovie, Ronald J.: Volume Ion Production Costs in Tenuous Plasmas: A General Atom Theory and Detailed Results for Helium, Argon, and Cesium. NASA TN D-4150, 1967.

26. Sovie, Ronald J.: Spectroscopic Determination of Electron Temperature and Percentage Ionization in a Helium Plasma. Phys. Fluids, vol. 7, no. 4, Apr. 1964, pp. 613-614.

27. Bechtel, Robert T.: Component Testing of a 30-Centimeter Diameter Electron Bombardment Thruster. Paper 70-1100, AIAA, Aug. 1970.

28. Kaufman, Harold R.: Ion-Thruster Propellant Utilization. Ph.D. Thesis, Dept. Mech. Eng., Colorado State Univ., 1971.

29. Kupriyanov, S. E.; and Latypov, Z. Z.: Ionization of Positive Ions by Electrons. Soviet Phys. - JETP, vol. 18, no. 2, Feb. 1964, pp. 558-559.

30. Varshavskii, S. P.; Mityureva, A. A.; and Penkin, N. P.: Effective Cross Sections for the Function of Excited Mercury Ions During Ionization of Mercury Atoms by Electron Impact. Optics and Spectrosc., vol. 28, no. 1, Jan. 1970, pp. 12-14.

31. Foster, E. W.: New Terms of the $5d^8 6s^2$ and $5d^8 6s6p$ Configurations of the Spectrum of Hg III. Proc. Roy. Soc. (London), Ser. A, vol. 200, no. 1062, Feb. 7, 1950, pp. 429-437.

32. Milder, Nelson L.: Comparative Measurements of Singly and Doubly Ionized Mercury Produced by Electron-Bombardment Ion Engine. NASA TN D-1219, 1962.

33. Rawlin, Vincent K.; and Kerslake, William R.: SERT II: Durability of the Hollow Cathode and Future Applications of Hollow Cathodes. J. Spacecraft Rockets, vol. 7, no. 1, Jan. 1970, pp. 14-20.

34. Frisch, S. E.; and Klucharyov, A. N.: The Role of Cascade Transitions in the Excitation of the $6s7s\,^3S_1$ Level of Mercury. Optics and Spectrosc., vol. 22, no. 2, Feb. 1967, pp. 92-94.

35. Hanle, W.; and Schaffernicht, W.: Measurements of the Light Yield in the Excitation of the Mercury Spectrum by Electron Collisions. Ann. d. Physik, vol. 6, Oct. 10, 1930, pp. 905-931.

36. Thieme, Otto: Lichtausbeute im Helium-, Quecksilber- und Stickstoffspektrum bei Anregung durch Electronensto β. Zeit. f. Physik, vol. 78, Oct. 4, 1932, pp. 412-422.

37. Lebedeva, V. K.; and Fabrikant, V. A.: Intensity Ratio in the Visible Mercury Triplet. Izvest. Akad. Nauk. SSSR, Ser. Fiz, vol. 19, 1955, pp. 7-8.

38. Schouten, J.: The Intensity Ratios of the Lines of the Mercury Triplet λ = 5461, 4358, and 4047 Å. Physica, 's Grav., vol. 10, Oct. 1943, pp. 672-678.

39. Jongerius, H. M.: Measurements of Optical Excitation Functions of the Mercury Atom (Excitation by Electrons). Philips Res. Rep. Suppl., No. 2, 1962.

NASA-Langley, 1971 —— 28 E-6469

"The aeronautical and space activities of the United States shall be conducted so as to contribute . . . to the expansion of human knowledge of phenomena in the atmosphere and space. The Administration shall provide for the widest practicable and appropriate dissemination of information concerning its activities and the results thereof."

— NATIONAL AERONAUTICS AND SPACE ACT OF 1958

NASA SCIENTIFIC AND TECHNICAL PUBLICATIONS

TECHNICAL REPORTS: Scientific and technical information considered important, complete, and a lasting contribution to existing knowledge.

TECHNICAL NOTES: Information less broad in scope but nevertheless of importance as a contribution to existing knowledge.

TECHNICAL MEMORANDUMS: Information receiving limited distribution because of preliminary data, security classification, or other reasons.

CONTRACTOR REPORTS: Scientific and technical information generated under a NASA contract or grant and considered an important contribution to existing knowledge.

TECHNICAL TRANSLATIONS: Information published in a foreign language considered to merit NASA distribution in English.

SPECIAL PUBLICATIONS: Information derived from or of value to NASA activities. Publications include conference proceedings, monographs, data compilations, handbooks, sourcebooks, and special bibliographies.

TECHNOLOGY UTILIZATION PUBLICATIONS: Information on technology used by NASA that may be of particular interest in commercial and other non-aerospace applications. Publications include Tech Briefs, Technology Utilization Reports and Technology Surveys.

Details on the availability of these publications may be obtained from:

SCIENTIFIC AND TECHNICAL INFORMATION OFFICE

NATIONAL AERONAUTICS AND SPACE ADMINISTRATION

Washington, D.C. 20546